Marine Structures 77 (2021) 102975

Contents lists available at ScienceDirect

Marine Structures

journal homepage: http://www.elsevier.com/locate/marstruc

Assessment of operational limits: Effects of uncertainties in sea state description

Lin Li [a,*], Sverre Haver [a], Nikita Berlin [b]

[a] Department of Mechanical and Structural Engineering and Materials Science, University of Stavanger, Stavanger, Norway
[b] Department of Offshore Oil and Gas Field Development, Gubkin Russian State University of Oil and Gas, Moscow, Russia

ARTICLE INFO

Keywords:
Allowable sea states
Operability
Wind sea and swell sea
Wave spectrum
Vessel heading
Lifting operation

ABSTRACT

For operations dominated by waves, operational limits are normally expressed in terms of allowable sea state parameters, such as the significant wave height (H_s) and spectral peak period (T_p). The allowable sea states need to be assessed in the planning phase of the operations. Different sources of uncertainties (including weather forecasts, wave spectral model and numerical models) should be accounted for in the allowable sea states to provide safety margins. This study focuses on assessment of the operational limits (in terms of H_s and T_p) considering the uncertainties associated with the sea state descriptions used in the numerical analysis. The aim is to demonstrate the effects of simultaneous description of wind sea and swell sea accounting for their different directional spreading and directions of propagation. A case study using lifting operation is chosen to address these uncertainties in the allowable sea states. To illustrate the results, two types of floating crane vessels, mono-hull and semi-submersible are employed in the case study. Operability analysis by using these vessels are performed and compared using NORA10 hindcast data for a site in the Barents Sea.

1. Introduction

Planning and execution of marine operations are integrated activities both in the process of designing marine structures and during the operational life of the structure. The installation of a structure at its target site at sea will involve several marine operations and the requirement established during planning of these operations may affect structural design. In this paper, we are not considering routine operations that are frequently done onboard as a part of the normal day to day operation. We will follow the DNVGL terminology that a marine operation is "a non – routine operation of a limited defined duration related to handling of object(s) and/or vessel(s) in the marine environment during temporary phases" [1].

As a first categorization, a marine operation can be defined as: i) weather restricted operation, or ii) unrestricted operation. The governing parameter for a weather restricted operation is its duration as established during planning. The planned duration must not exceed the horizon of a reliable weather forecast, which is typically taken to be 72 h. All marine operations with a planned duration beyond 72 h should be considered as an unrestricted operation. For an unrestricted operation, a standard ULS (ultimate limit state) design control for the operation, i.e., the characteristic load effects should be taken as the value corresponding to an annual exceedance probability of 10^{-2} for the given season. For a weather restricted operation, the design requirements will be much milder. A possibility that should be considered for an unrestricted operation is to consider if the operation can be divided into shorter sub-operations with

* Corresponding author.
E-mail address: lin.li@uis.no (L. Li).

https://doi.org/10.1016/j.marstruc.2021.102975
Received 6 November 2020; Received in revised form 19 January 2021; Accepted 9 February 2021
Available online 25 February 2021

each sub-operation fulfilling the requirement as for a weather restricted operation. However, it is important to ensure that for the condition between the sub-operations, the safety of the temporary operation state should not be worse than that before the operation started.

In this study, we consider a generic weather restricted operation. Operational limits need to be assessed during planning of marine operations. The limits can be expressed in terms of environmental conditions or motions that can be monitored on-board the installation vessels. The operational limits depend on the type of operation and the characteristics of the dynamic system. The operational limits can be used to improve the system performance in the planning phase, and they can also be used together with the weather forecasts to support on-board decision making in the execution phase [2]. Traditionally, operational limits have relied mostly on practical marine operation experiences. However, it is important to quantify the responses (forces, motions) and corresponding operational limits for complicated operations with strict requirements. A systematic method to establish the operational limits is required. Li (2016) and Guachamin-Acero et al. (2016) established a general methodology to establish the operational limits [3,4]. This general methodology uses response-based criteria to determine the allowable limits of sea states and to assess the safety of the operation. The operation is considered to be safe if the characteristic value of the governing response is less than the design capacity. Regarding examples of application of the general methodology and assessment of operational limits, reference is made to Refs. [5–7].

Often, safety factors need to be implemented to account for different sources of uncertainties in the operational limits. The alpha factors are recommended by DNVGL (2016) and ISO (2015) to account for uncertainties in weather forecasts by reducing the H_s limits [1,8]. They depend on the operation duration, the level of the initial H_s limits and whether meteorologists or measurement equipment are available on site. Alpha factors are only implemented in terms of H_s limits. Uncertainties in both H_s and T_p of the forecasts can be assessed by evaluating the error distributions between the forecasted wave characteristics and the hindcasted or measured wave characteristics [9–11].

Besides the wave parameters (H_s and T_p), the spectral shape also influences the predicted dynamic responses of the floating systems. Often, analytical wave spectra are applied to predict the motions of the installation system, such as the Joint North Sea Wave Project (JONSWAP) and the Pierson-Moskowitz (PM) wave spectral models [12,13]. For many situations, particularly moderate and low sea states, the sea states are combination of more than one wave system. Sea state including both a wind sea system and swell sea system can have a significant impact on the operability of floating offshore structures. Several models of combined sea states have been proposed, including the Ochi Hubble spectrum and the Torsethaugen spectrum [14,15]. It is important to consider the wind sea and swell sea components separately for sea state sensitive marine operations. To quantify the influences on the operational limits due to difference between spectra in the real ocean and those used in the numerical analysis, Guachamin-Acero and Li (2018) proposed a methodology to include the uncertainties related to the wave spectral shape in the operational limits (H_s and T_p) [16]. The methodology applied the directional hindcast wave spectra and dynamic numerical models.

For marine operations involving floating systems, it is important to assess the operational limits by considering uncertainties associated with how the short-term sea states are modelled in the numerical analysis during the planning phase. Therefore, the aim of this study is to perform comprehensive sensitivity studies on the allowable sea states in terms of H_s and T_p by using different models of the wave spectra. A lifting operation is chosen as a case study, and the vertical crane tip motion is considered as the most critical parameter to derive the allowable sea states. Frequency-domain analyses are applied based on linear assumptions. The influence of wave spreading, wave spectral type, and the direction misalignment of wind sea and swell sea on the allowable sea states are compared and discussed by using two types of installation vessels. Operability analysis are performed for two vessel types using hindcast data for a reference site in the Barents Sea.

2. Methodology

In this study, the example operation is lifting a sub-structure from the deck of the installation vessel using the crane of the vessel and lowering it to the sea bottom. The operation may involve several phases, but this study focuses on the most critical phase regarding the structural loading. The duration of the operation is taken to be 3 h. The vertical crane tip motion during the lowering phase is considered as the most critical parameter.

For given sea state and vessel heading, linear theory is used to establish the distribution of the 3-h extreme value for the crane tip vertical motions. Safety of operation is taken to be jeopardized if the amplitude of the vertical crane tip motion is too high. The operational criterion requires that the probability for the 3-h extreme value to exceed the limiting value should be less than a target probability. Thus, the permissible maximum H_s for given T_p can be found by fulfilling this criterion.

2.1. Crane tip response spectrum

The hydrodynamic properties of a floating vessel, including added mass, damping and excitation forces for different headings across the relevant frequency range can be calculated using potential flow theory. Then, the transfer functions of the vessel rigid motions can be obtained. The transfer function, $H_i(\omega,\theta)$, for the ith degree of freedom (DoF) can be expressed in complex form as shown in Eq. (1).

$$H_i(\omega,\theta) = A_i(\omega,\theta)\exp(i\phi_i(\omega,\theta)) \tag{1}$$

where ω is angular frequency; θ is the wave direction of propagation relative to the vessel; $A_i(\omega,\theta)(m/m)$ and $\phi_i(\omega,\theta)$ are response amplitude per unit wave amplitude and phase angle, respectively. The absolute value of the complex transfer function is the response

amplitude operator (RAO) of the vessel motion. For lifting operations, the crane tip motions are critical and influence the operability. The crane tip vertical motion, z_c, is used as main criterion to assess the operability, and depends on the heave, roll and pitch motions of the vessel, η_{3-5}. Assuming the crane tip location is (x_p, y_p, z_p) in the vessel fixed coordinate system, z_c is formulated as follows:

$$z_c = \eta_3 + y_p\eta_4 - x_p\eta_5 = \left[H_3(\omega,\theta) + y_pH_4(\omega,\theta) - x_pH_5(\omega,\theta)\right]\cdot\zeta_a \tag{2}$$

where ζ_a is wave amplitude. The RAO for the vertical crane tip motion, $RAO_{Z_c}(\omega,\theta)$, is the absolute value of the transfer function for the vertical motion of the crane tip, $H_{Z_c}(\omega,\theta)$, which can be expressed as follows:

$$RAO_{Z_c}(\omega,\theta) = |H_{Z_c}(\omega,\theta)| = \left|H_3(\omega,\theta) + y_pH_4(\omega,\theta) - x_pH_5(\omega,\theta)\right| \tag{3}$$

Knowing the RAO, the response spectrum of the vertical crane tip motions for long-crested wave propagating in the main direction, θ_0, is as follows:

$$S_{Z_c}(\omega,\theta_0) = (RAO_{Z_c}(\omega,\theta_0))^2\cdot S(\omega) \tag{4}$$

where $S(\omega)$ is the long-crested wave spectrum. The spectral moments for the response spectrum, m_k can be obtained:

$$m_k = \int_0^\infty \omega^k\cdot S_{Z_c}(\omega,\theta_0)d\omega \tag{5}$$

The statistical parameters, including the standard deviation (STD), σ_{Z_c}, the averaged zero-up-crossing period, T_z, as well as the average number of response cycles in 3 h, N_{3h}, for the given wave direction, θ_0, can be estimated from the response spectrum.

$$\sigma_{Z_c} = \sqrt{\int_0^\infty S_{Z_c}(\omega,\theta_0)d\omega} \tag{6}$$

$$T_z = 2\pi\cdot\sqrt{\frac{m_0}{m_2}} \tag{7}$$

$$N_{3h} = \frac{10800}{T_z} \tag{8}$$

These statistical parameters will be used for assessment of the allowable sea states for long-crested wave conditions. The commonly used wave spectral types on the Norwegian Continental Shelf are discussed in Appendix A.1.

For short-crested waves with wave spectrum $S(\omega,\theta)$ (see Appendix A.2), we can re-write the response spectrum as functions of both direction θ and frequency ω as follows:

$$S_{Z_c}(\omega,\theta) = (RAO_{Z_c}(\omega,\theta))^2\cdot S(\omega,\theta) \tag{9}$$

The spectral moments, m_k, and standard deviation σ_{Z_c}, should thus be integrated with respect to both θ and ω:

$$m_k(\theta_0) = \int_{\theta_0-\frac{\pi}{2}}^{\theta_0+\frac{\pi}{2}}\int_0^\infty \omega^k\cdot S_{Z_c}(\omega,\theta)d\omega d\theta \tag{10}$$

$$\sigma_{Z_c}(\theta_0) = \sqrt{\int_{\theta_0-\frac{\pi}{2}}^{\theta_0+\frac{\pi}{2}}\int_0^\infty S_{Z_c}(\omega,\theta)d\omega d\theta} \tag{11}$$

where $\theta_0 \mp \frac{\pi}{2}$ are the lower and upper spreading directions corresponding to the mean wave direction, θ_0. Typically, θ_0 is different for wind sea and swell sea.

2.2. Operational criterion and allowable sea states

Heavy lift operations are often performed in relatively calm weather, where linear wave theory can be used to describe the waves and the vessel motions. For a limited duration, say 3 h, the involved processes (surface elevation and vessel motions), can be reasonable well modelled as stationary Gaussian processes. Provided these processes are strictly narrow banded, the global maxima (largest maximum between adjacent zero-up-crossings) of the vertical crane tip motion follow the Rayleigh distribution [17]. In practice, neither surface elevation process nor response processes are strictly narrow banded. However, provided that the processes are **not** strictly broad banded (white noise) which will be fulfilled for most practical cases, the Rayleigh distribution will be a valid model for predicting large extremes if the focus is on global maxima (global maximum: largest maximum between adjacent zero-up-crossings)

and target exceedance probability are calculated in terms of the mean zero-up-crossing period [18].

For lifting operations, the maximum vertical motion of the crane tip in 3 h, Z_{3h}, can be used as the critical parameter for the operation. By further assuming that the global maxima are statistically independent and identically distributed, the distribution of Z_{3h} can be expressed as Eq. (12).

$$F_{Z_{3h}}(z) = \left\{1 - exp\left\{-\frac{1}{2}\left(\frac{z}{\sigma_{Z_c}}\right)^2\right\}\right\}^{N_{3h}} \tag{12}$$

The present choice of 3 h' duration is somewhat arbitrary. In practice, the target safety level for an operation will be specified per operation with expected duration. But the acceptable target failure probability for any duration can be converted into the acceptable target failure probability per 3 h. Here we refer to target safety in term of a maximum permissible failure in 3 h denoted q_{3h}.

To find the suitable limiting sea states, it is reasonable to require that the probability of the 3-h maxima exceeding the limiting value, z_{lim}, should be less than the selected target probability, q_{3h}. To satisfy this, the following equation should be fulfilled:

$$P[Z_{3h} > z_{lim}] = 1 - \left\{1 - exp\left\{-\frac{1}{2}\left(\frac{z_{lim}}{\sigma_{Z_c}}\right)^2\right\}\right\}^{N_{3h}} \leq q_{3h} \tag{13}$$

From Eq. (13), a limiting value for the standard deviation (STD) of the vertical crane tip motion, $\sigma_{Z_c,lim}$, can be calculated:

$$\sigma_{Z_c} \leq \sigma_{Z_c,lim} = \frac{z_{lim}}{\sqrt{-2\ln\left[1 - (1 - q_{3h})^{1/N_{3h}}\right]}} \tag{14}$$

For different sea states with spectral parameters in terms of H_s and T_p, the allowable sea states can be established by comparing the STD values of the vertical crane tip motions calculated from Eq. (6) and Eq. (11) for long-crested and short-crested seas, respectively, with the limiting value from Eq. (14).

3. Case study

3.1. Installation vessels

Two floating crane vessels, a mono-hull and a semi-submersible are employed in the case study. The hull shapes of the two crane vessels are indicated in Fig. 1 and the main characteristics are listed in Table 1. The mono-hull vessel is a typical heavy lift vessel for different offshore installation activities. The crane is able to perform lifting operation of up to 5000 tons at an outreach of 32 m. The semi-submersible vessel has two fully submerged longitudinal pontoons, and they are connected to the main deck by six vertical columns. The lifting capacity of the crane is over 10,000 tons. The displaced volume of the mono-hull vessel is about 40% of the semisubmersible vessel. Both the semi-submersible vessel and the mono-hull vessel are equipped with dynamic positioning systems to keep the vessels in position. Analyses of lifting operations using these two crane vessels can be found in Refs. [20,21].

The crane tip position of the vessels depend on the practical arrangement of the lifting operations. In this study, we assume that both vessels are performing heavy lift operations with the crane tip at 80 m height. The lifting positions are assumed to be close to the mid-ship in longitudinal direction, and the coordinates of the crane tip in the transverse direction are chosen to ensure sufficient clearance between the lifted object and the hull of the vessels. Thus, the crane tip position for the semi-submersible has a larger coordinate in transverse direction compared to the mono-hull due to the larger breadth.

The eigenvalues of the floating vessels are evaluated in the frequency domain, without including any external forces or damping effects. The undamped natural periods can be obtained by solving the following equation:

$$\left[-\omega^2(\boldsymbol{M} + \boldsymbol{M}_\infty) + \boldsymbol{K}\right] \cdot \boldsymbol{x} = 0 \tag{15}$$

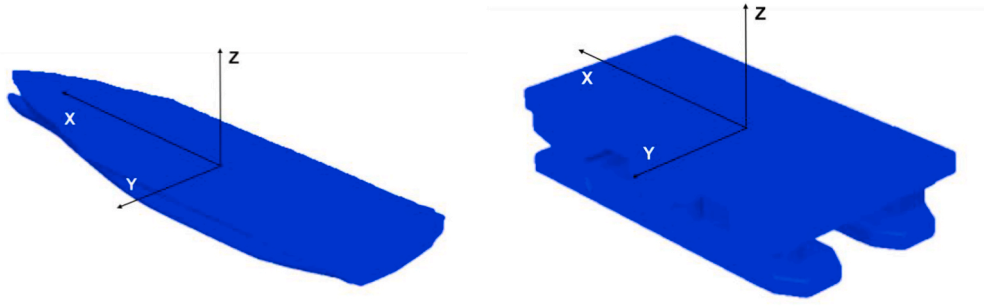

(a) Mono-hull (b) Semi-submersible

Fig. 1. Hull shapes of two floating installation vessels for the case study.

Table 1
Main parameters for the two floating crane vessels.

Parameters	Unit	Mono-hull	Semi-submersible
Length	(m)	183	175
Breadth	(m)	47	87
Operational draft	(m)	12	26.1
Displacement	(tons)	6.3E4	1.7E5
Crane tip position	(m)	(-10.5, 53.5, 80)	(-10.5, 70, 80)

Table 2
The natural periods (s) (and natural frequencies in rad/s) of the vessel motions.

Vessel	Surge	Sway	Heave	Roll	Pitch	Yaw
Mono-hull	87.3	75.2	10.6 (0.59)	13.7 (0.46)	9.4 (0.67)	85.7
Semi-submersible	83.7	75.3	22.2 (0.28)	22.8 (0.28)	17.2 (0.37)	86.7

where ω is natural frequency; $\boldsymbol{M}$ and $\boldsymbol{M}_{\infty}$ are mass matrix and the added mass matrix at infinite frequency, respectively; $\boldsymbol{K}$ is the stiffness matrix including hydrostatic restoring and equivalent stiffness from the positioning system. $\boldsymbol{x}$ is the motion vector. By solving the eigenvalue problem, the natural periods of the two installations vessels are presented in Table 2. For lifting operations, which are sensitive to the crane tip vertical motions, the vessel motions in the vertical plane (heave, roll and pitch) are of most concern. The response amplitude operators (RAOs) of the vessels have been calculated using potential flow solver WADAM [22], from which the hydrodynamic properties are obtained based on the panel method in the frequency domain. Fig. 2 presents the RAOs of the two vessels in heave, roll and pitch for three wave directions.

As clearly shown in Table 2, the natural periods of the mono-hull vessel motion in heave, roll and pitch are between 9s and 14s, which are within typical wave period of swell seas when focusing on low sea states. The natural periods of the semi-submersible vessel are above 17s, which are longer than typical period of swell sea at least in summer seasons. The peaks of the RAOs in Fig. 2 for different vessel motions also correspond well to the natural periods for different vessel motions. For both vessels, the RAOs are highly dependent of the wave directions. The beam sea condition (90 deg) will result in significant higher roll and heave motions compared to those under head sea condition (180 deg) for both vessels. The highest RAO value in roll for the mono-hull under beam sea condition is around three times higher as that for the semi-submersible. The strong couplings between heave and pitch for the semi-submersible are observed, where multiple peaks in heave and pitch are displayed.

The different behavior of the RAOs of the two vessels introduces different responses of the crane tip under various conditions and

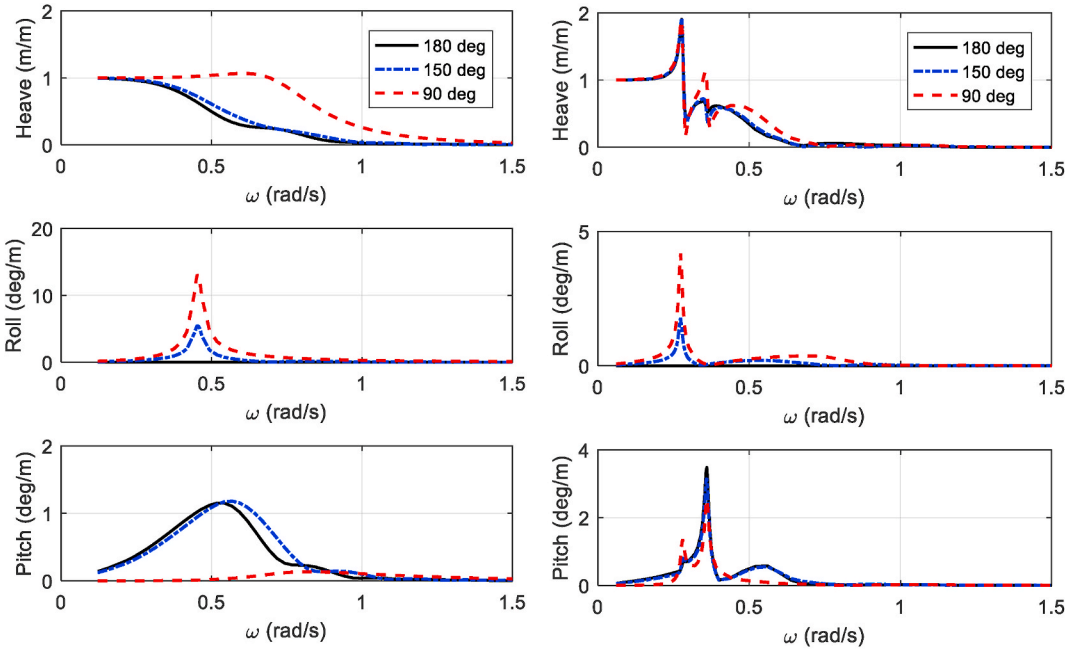

Fig. 2. RAOs of the two crane vessels for three wave directions.

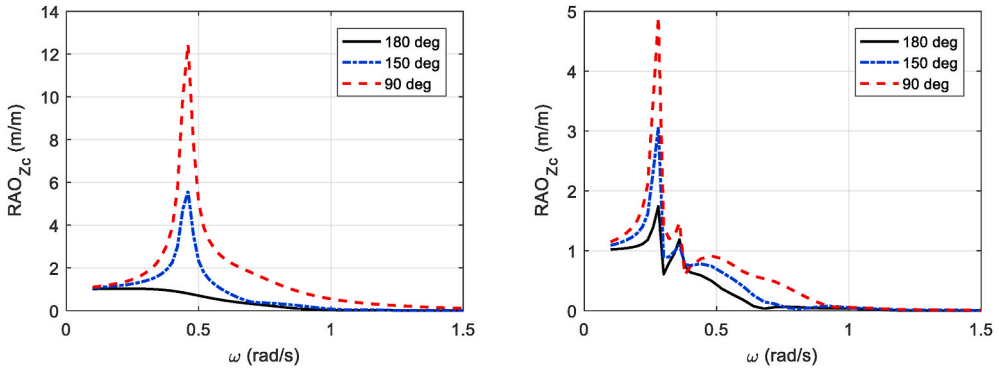

Fig. 3. RAOs of the crane tip vertical motion of the two crane vessels.

thus result in different allowable sea states for the lifting operations. By following Eq. (3), the RAOs of the vertical crane tip motions at the given tip positions (see Table 1) are obtained and presented in Fig. 3. As expected, the beam sea conditions introduce the highest crane tip motions among all directions for both vessels. The frequencies of the peak values correspond to the eigenfrequencies in roll. For typical wave frequency range between 0.5 and 1 rad/s, the crane tip vertical motions increases with decreasing wave frequencies, indicating more severe motions in longer waves. In the swell frequency range, the mono-hull vessel experiences much higher RAOs compared to the semi-submersible vessel.

3.2. Operational criterion

Different approaches can be used for analysis of lifting operations. For operations with complex geometry and non-linear hydrodynamic forces, time-domain simulations are required to obtain the responses of the lifting system. For preliminary assessment of operational limits and operability during the initial planning phase of a marine operation, simplified methods can be applied based on the recommend practice [23].

In this study, we focus on the influence of the spectral type of the wind sea and swell sea components on the operational limits. Obtaining the critical responses by screening of all possible sea states is required, which makes time-domain simulations impractical. Therefore, we use simplified method by assuming that the responses of the lifted object are dominated by the vertical motion of the crane tip. The characteristic vertical crane tip motions can be used as operational criterion and found by using frequency-domain methods [23].

The maximum vertical motion of the crane tip in 3 h is chosen as the critical parameter for the lifting operation. A limiting value, $z_{lim} = 0.5\ m$, together with a limiting target probability of exceedance, $q_{3h} = 0.0001$, are applied to assess the operational limits, i.e. the probability of a vertical crane tip motion exceeding 0.5 m during 3 h should be less than 0.0001. The limiting standard deviation of vertical crane tip motion, $\sigma_{Z_{c,lim}}$, can be calculated based on this criterion following Eq. (14). By screening different H_s and T_p conditions, the allowable sea states can be established by comparing the STD values with the limiting value, $\sigma_{Z_{c,lim}}$.

4. Assessment of allowable sea states

The allowable sea states in terms of H_s and T_p are presented in this section. The influence of wave spreading, wave spectral type, as well as direction misalignment of wind sea and swell sea on the allowable sea states are discussed.

4.1. Long-crested waves

The allowable sea states under long-crested waves are evaluated by using JONSWAP and Torsethaugen spectra (see discussions on wave spectral types in Appendix A.1). The response spectra of the vertical crane tip motions under two different spectral peak periods are compared for the two vessels in Fig. 4.

In short wave conditions ($T_p = 6\ s$), the response spectra using Torsethaugen wave spectrum represent much higher spectral density than using JONSWAP wave spectrum for both vessels. As discussed, the swell sea is expected to have a period around 10s using the two-peak spectrum when the wind sea peak period of 6 s. For JONSWAP spectrum, the wave spectrum is concentrated around 6 s. Moreover, the RAOs of the vertical crane tip motion are peaked around 12 s for the mono-hull and have large values for waves longer than 12 s for the semi-submersible (see Fig. 3). Because of this, additional response variance is seen around 12 s using Torsethaugen spectrum compared to what is obtained using JONSWAP with peak period around 6 s. When $T_p = 12\ s$, the response spectra have peaks around 12 s using both wave spectra. The response variance is larger for both spectra compared to $T_p = 6\ s$. Moreover, the peaks are lower using Torsethaugen than using JONSWAP when $T_p = 12\ s$, because using Torsethaugen spectrum spreads spectral densities to the wind sea component with lower spectral peak period.

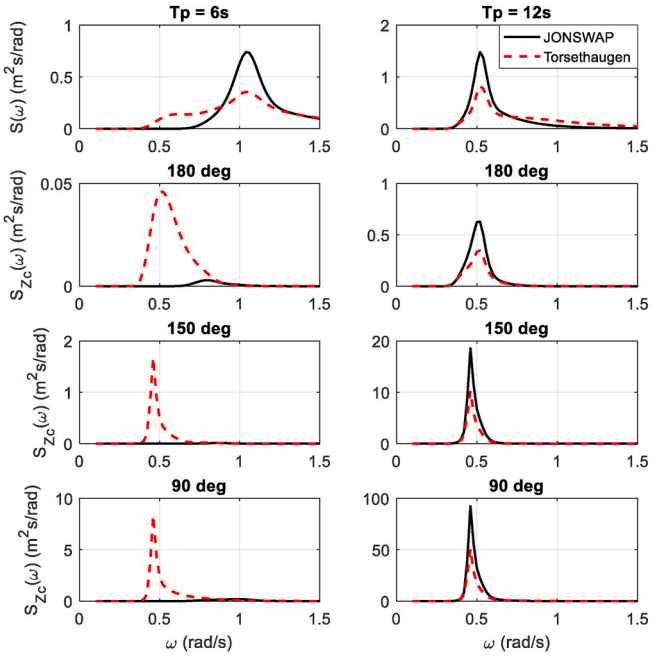

(a) Mono-hull

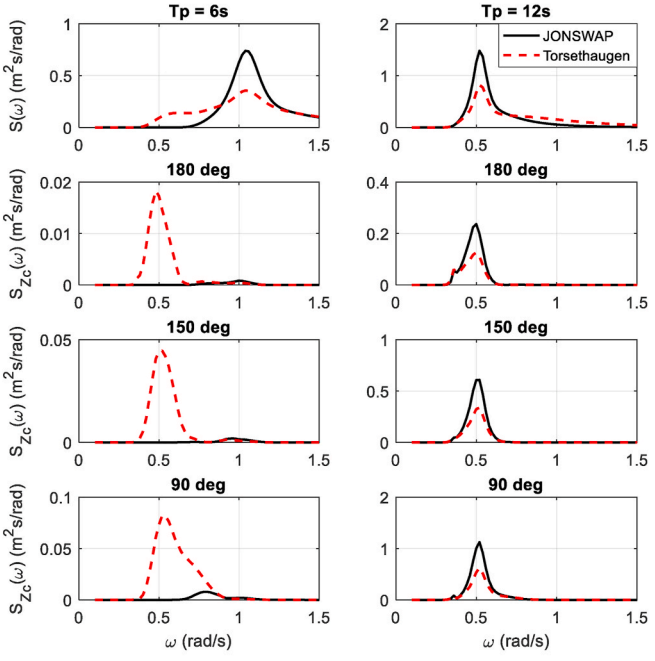

(b) Semi-submersible

Fig. 4. Response spectra for the vertical crane tip motion of the two crane vessels ($H_s = 2\,m$, long-crested wave).

When comparing the response spectra using the two vessels, the spectral density is in general higher for the mono-hull than the semi-submersible, especially in the short wave condition ($T_p = 6s$). These observations are consistent with the RAOs of the vertical crane tip motions. For both vessels, the density of response spectra increases when the wave direction changes from the head sea to the beam sea.

By screening the possible wave conditions, the allowable sea states using long-crested waves are obtained and presented in Fig. 5. Obviously, the allowable H_s values are significantly lower using Torsethaugen spectrum in wave conditions with T_p less than 9 s for all cases. When the wind sea component is dominant with T_p less than 9 s, the Torsethaugen spectrum gives a secondary peak corresponding to swell sea component with larger T_p. This swell sea adds variance to the crane tip response that is missing using the single-peak JONSWAP spectrum. On the other hand, the JONSWAP spectrum only has one peak, and the allowable H_s decrease rapidly with increasing T_p. For very long wave condition with T_p larger than 12 s, it is observed that the allowable H_s values are higher using Torsethaugen spectrum. This is consistent with the response spectra shown in Fig. 4 and is due to that part of the wave variance energy is shifted to short wave components with Torsethaugen spectrum. Furthermore, as the RAOs of the vertical crane tip motions are greatly influenced by the vessel roll motions, the allowable H_s values drop greatly when the wave direction moves away from the head seas.

Because of the better performance of the semi-submersible vessel, the allowable sea states are higher than those using the mono-hull vessel. The highest H_s values of the semi-submersible vessel are around 3 m (180 deg & $T_p = 9$ s) using Torsethaugen spectrum, which is 1 m higher than that of the mono-hull vessel. These differences will result in significant deviations in the operability of the two vessels. It should be noted that the operations are often carried out with wave directions close to the heading sea condition. However, the allowable sea states under sea beam sea condition are presented in this study for a better comparison.

4.2. *Influence of short-crested seas*

As discussed in Appendix A.2, real ocean waves spread into different directions of propagation, especially for wind seas. When using long-crested waves, the influence of the roll motion on the crane tip response can be minimized by heading to the waves (180 deg). However, when the waves are short-crested, the contributions from other wave directions also need to be considered. Fig. 6 presents the 3D response spectra for the crane tip motion for the chosen sea state. Spreading index n of 2 and 10 for short-crested waves are compared for two wave spectra.

When the wave spreading is high ($n = 2$), the spectral density is distributed over a larger range of directions compared to $n = 10$ for

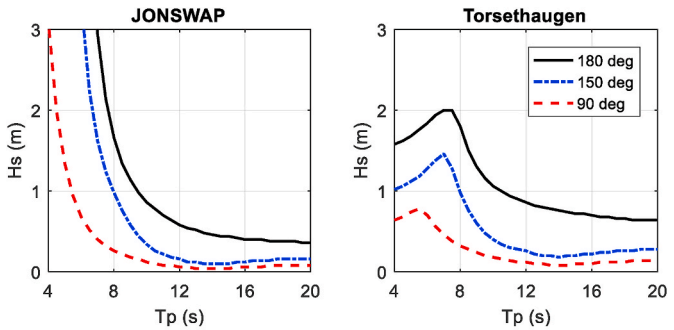

(a) Mono-hull

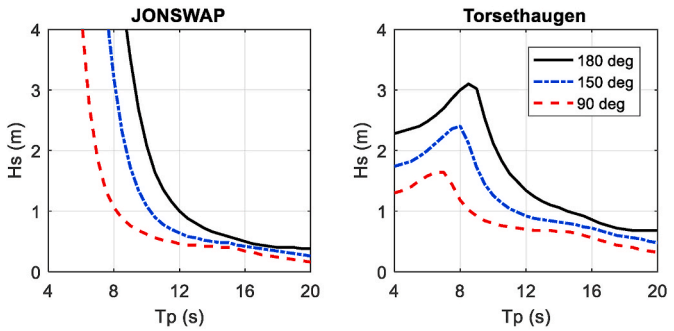

(b) Semi-submersible

Fig. 5. Allowable sea states using long-crested waves.

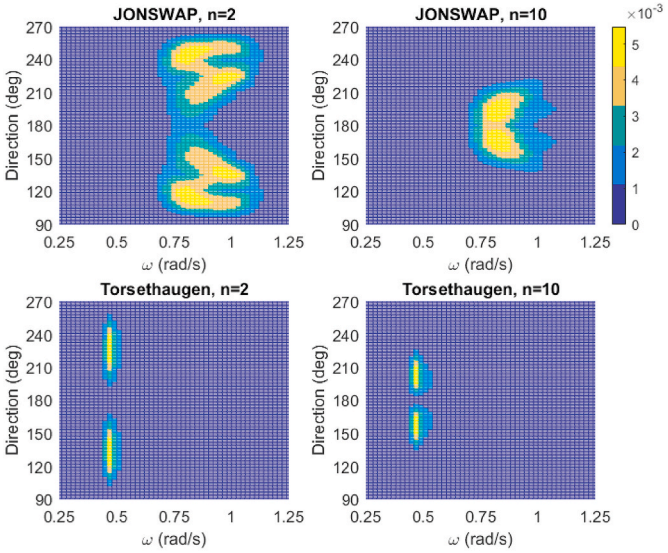

(a) Mono-hull

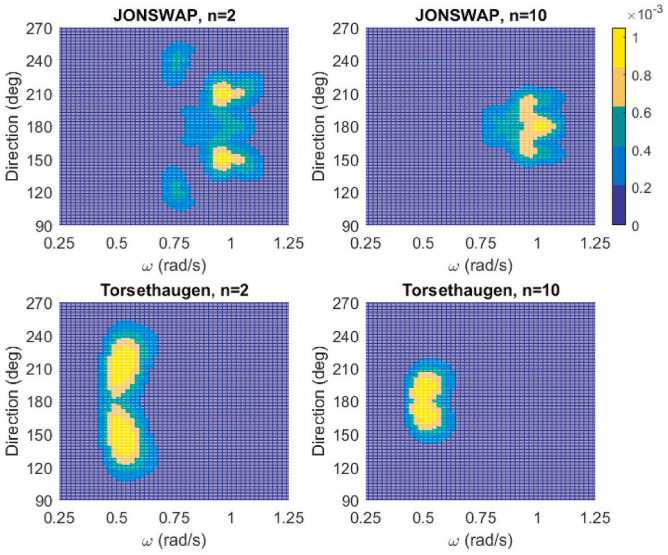

(b) Semi-submersible

Fig. 6. Response spectra for the crane tip vertical motion, $S_{Z_c}(\omega, \theta)$, for short-crested wave conditions ($H_s = 2\,m$, $T_p = 6\,s$, main wave direction 180 deg).

both vessels and both spectral types. Although the wave spectrum is most powerful at 180 deg, the response spectral density is highest close to 110–135 deg and 225–250 deg since the RAO values are much higher close to beam seas for the mono-hull vessel. For the semi-submersible vessel, the highest response density appears around 150 deg and 210 deg.

Similar to the long-crested wave condition, the 3D response spectra also display that the spectral density distributions across the wave frequency are rather different using JONSWAP and Torsethaugen spectra. While the response spectrum is peaked close to 7–8 s using JONSWAP, the energy is concentrated to close to 14 s using the two-peak spectrum for mono-hull. For the semi-submersible, the spectral density is peaked close to 6 s using JONSWAP and close to 12 s using Torsethaugen spectrum. When using Torsethaugen, the spectral densities are spreading over a broader frequency range for the semi-submersible. This is because the crane tip RAOs for the mono-hull has one high peak value around 14 s, which is close to the second peak of the wave spectrum. However, the RAOs values are between 0.5 and 1 for a broader wave period range between 9 and 15 s for semi-submersible.

As the wave spreading has great influence on the responses, it is important to study their effects on the allowable sea states. Fig. 7 compares the allowable sea states for two wave directions using three different spreading indices. Both JONSWAP and Torsethaugen spectra are applied for each vessel type. For both vessels, the influence of the wave spreading on the sea states have similar trend. When wave direction is 180 deg, including the spreading of the waves decrease the sea states. The decrease is more significant for the mono-hull vessel. Thus, if the wave spreading is not considered properly, the operability may be greatly over-estimated.

4.3. Influence of direction misalignment of wind seas and swell seas

In the previous subsections, both single-peak and double-peak wave spectra are considered when assessing the allowable sea states. For the double-peak wave spectrum, both wind sea and swell sea components are represented. Moreover, when using Torsethaugen spectrum formulation, both wind sea and swell sea components are assumed to have the same wave direction. In real offshore conditions, however, the two components will typically propagate in different directions relative to the structures. The spreading of the two components are usually different as well. While wind sea often has spreading index around $n > 2-4$, swell sea are more concentrated around its main direction with $n > 8$. What is governing for swell spreading index is whether the swell sea represents incoming swell from a remote storm, or it represents decaying wind sea in target area due to a large shift in wind direction. Thus, it is useful to decompose the two wave components and examine the influence of the misalignment angle on the allowable sea states. Sensitivity of response to spreading indices do also represent sources of uncertainties, in particular for the swell sea.

As shown in Fig. 21 (see Appendix A.1), the Torsethaugen spectrum can be decomposed into two JONSWAP wave spectra, representing wind sea and swell sea components, respectively. Here, for a given total H_s and T_p, we split the two wave components and apply different directions and spreading indices. $n = 2$ and 10 are applied as spreading indices for wind sea and swell sea components, respectively. Fig. 8 displays the 3D wave spectrum for one total sea condition with two wave components propagating in different directions. As clearly seen, the wind seas have more directional spreading compared to the swell sea. The resulting 3D response spectra for the vertical crane tip motions are shown in Fig. 9 for both installation vessels.

When the wind sea and swell directions are misaligned, the response spectrum tends to concentrate the energy around the swell sea

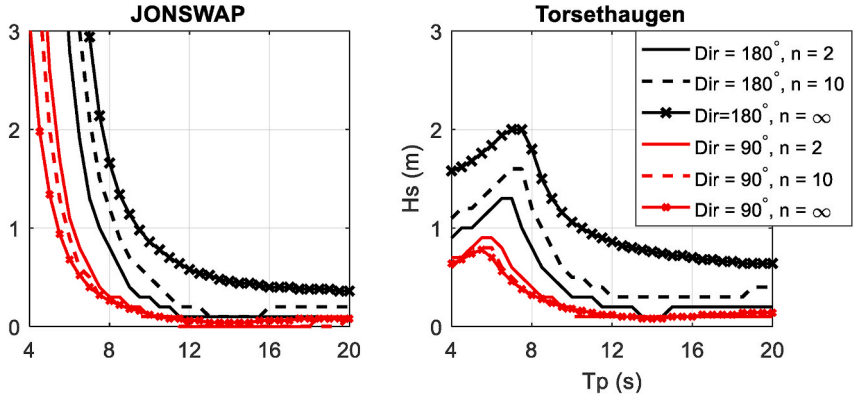

(a) Mono-hull

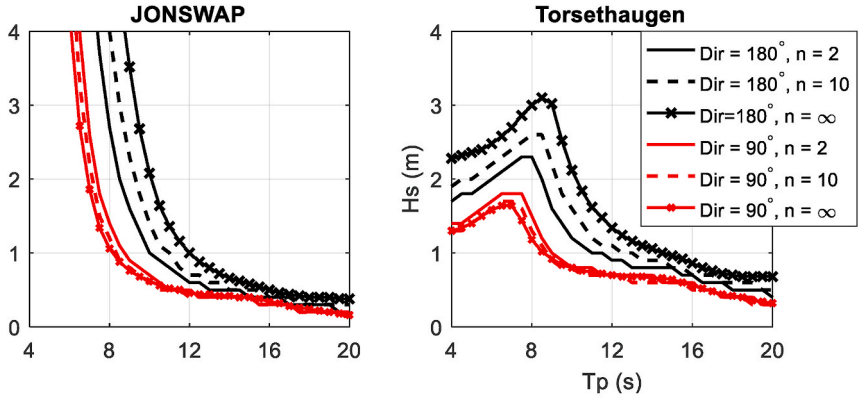

(b) Semi-submersible

Fig. 7. Allowable sea states with different spreading index for short-crested waves.

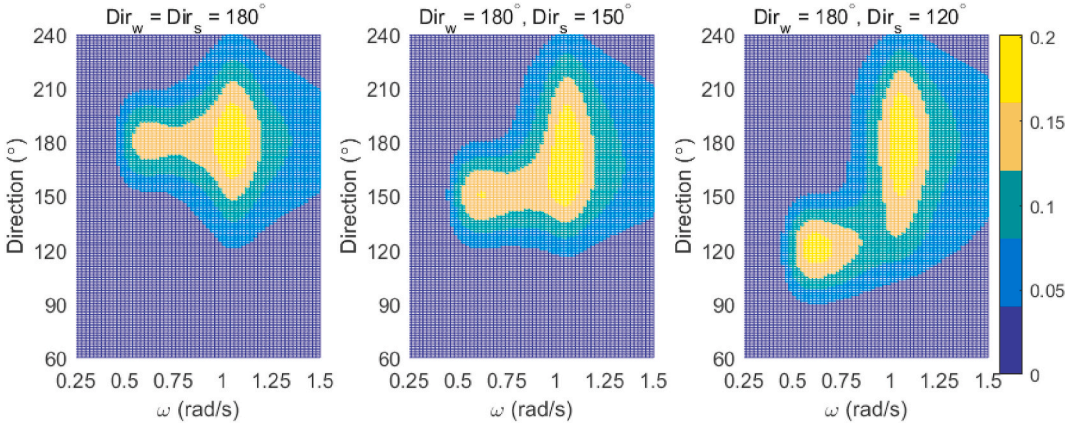

Fig. 8. Wave spectra with separate wind sea and swell sea components (total sea: $H_s = 2\,m$, $T_p = 6\,s$; wind sea component: $H_{s1} = 1.69\,m$, $T_{p1} = 6\,s$, $n_1 = 2$; swell sea component: $H_{s2} = 1.06\,m$, $T_{p2} = 10.3\,s$, $n_2 = 10$).

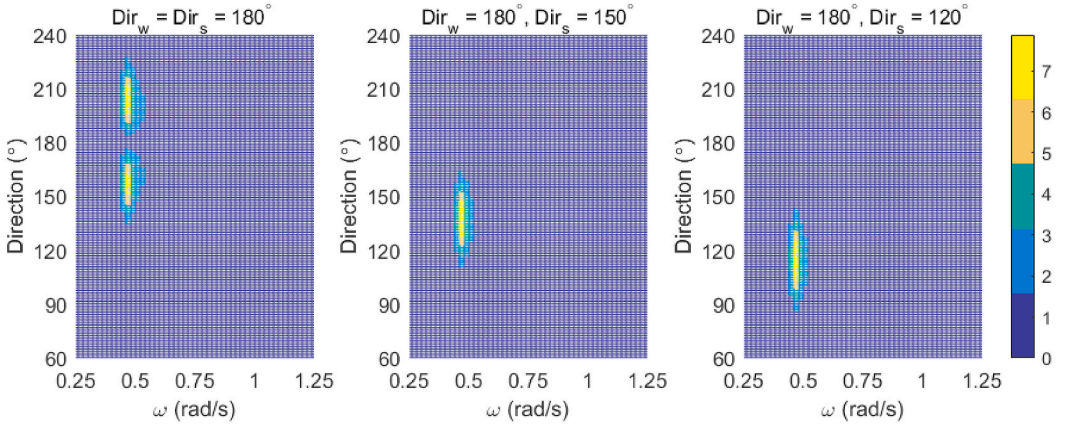

(a) Mono-hull

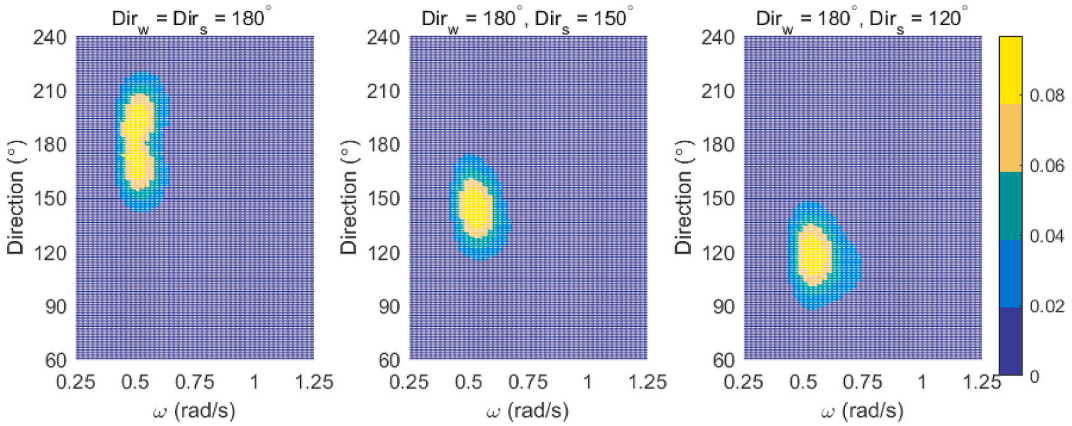

(b) Semi-submersible

Fig. 9. Response spectra for the crane tip vertical motion, $S_{Z_c}(\omega,\theta)$, with misaligned wind sea and swell sea (total sea: $H_s = 2\,m$, $T_p = 6\,s$; wind sea component: $H_{s1} = 1.69\,m$, $T_{p1} = 6\,s$, $n_1 = 2$; swell sea component: $H_{s2} = 1.06\,m$, $T_{p2} = 10.3\,s$, $n_2 = 10$).

Table 3
Standard deviations (m) of the vertical crane tip motion corresponding to the cases in Fig. 9 (total sea $H_s = 2\,m$, $T_p = 6\,s$).

Vessel type	Headings of wind sea and swell sea components (deg)		
	180, 180	180, 150	180, 120
Mono-hull	0.228	0.370	0.610
Semi-submersible	0.071	0.089	0.118

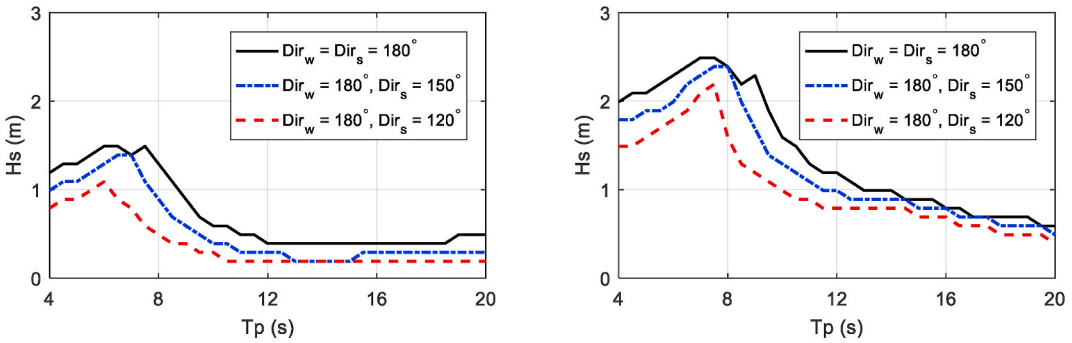

(a) Mono-hull (b) Semi-submersible

Fig. 10. Allowable sea states with misaligned wind seas and swell seas.

directions. This is because the crane tip motion RAOs have higher values close to the T_p of the swell sea component. When the swell moves from the 180 towards 120 direction, the total density of the response spectra increases with increasing misalignment angle because of the increasing RAO as the directions moves towards beam seas. The STD values of the corresponding response spectra can be found in Table 3.

Because of the direction misalignment of wind sea and swell sea components, the allowable sea states decrease compared to the aligned conditions. The resulting sea states for both vessels are compared in Fig. 10. For wave conditions with T_p less than 10 s, the misalignment can cause a 20–50% decrease of the limiting allowable H_s values for both vessels, indicating a potential huge influence on the operability. However, the operability for a given site condition depend greatly on the relative wave height and directions between the wind sea and swell sea components.

4.4. Discussions on the uncertainties in the allowable sea states

It has been shown that the allowable sea states depend on the sea state modelling methods with parameters including wave spectral type, spreading, and direction misalignment between the wind sea and swell sea components. During the planning phase of an operation, it is important to choose representative parameters and provide the allowable sea states that will be used during the execution phase. Because of the differences between the modelled sea states in the numerical analysis and those in the real conditions, uncertainties on the allowable sea states do exist. These uncertainties reflect that the operational limits may be over- or under-estimated by the numerical analysis. Thus, it is essential to include different sources of uncertainties during both the planning and execution phases to increase the safety level of the operations.

The commonly used engineering approach only applies alpha factors to consider the uncertainties in the weather forecasts as recommended by DNVGL and ISO [1,8]. Moreover, the numerical analyses during the planning phase are often simplified to some extent, and sensitivity studies on the sea state modelling parameters are not comprehensively implemented. Because of this, it is important to discuss the uncertainties in the allowable sea states and assess whether alpha factors can cover these uncertainties. Three cases are selected as below for comparisons:

a) Base case, for which the sea state is modelled using long-crested JONSWAP spectrum with a wave direction of 160 deg. This case represents the commonly used simplified engineering approach. As suggested by DNVGL [23], when long-crested sea is applied for simplicity, a heading angle of $\pm 20^\circ$ is recommended to account for the additional effect from short-crested sea.
b) Case 1, for which the sea state is modelled by short-crested ($n = 2$) JONSWAP spectrum with a wave direction of 180 deg. This case represents the wind sea condition with a significant degree of directional spreading.
c) Case 2, for which the sea state includes both wind sea (short-crested with $n = 2$ and a direction of 180 deg) and swell sea (short-crested with $n = 10$ and a direction of 150 deg). The direction misalignment between the wind sea and swell sea components is also considered in order to represent a more realistic and complicated sea condition.

The allowable sea states for the above three cases are obtained for both the mono-hull and semi-submersible vessels, as shown in

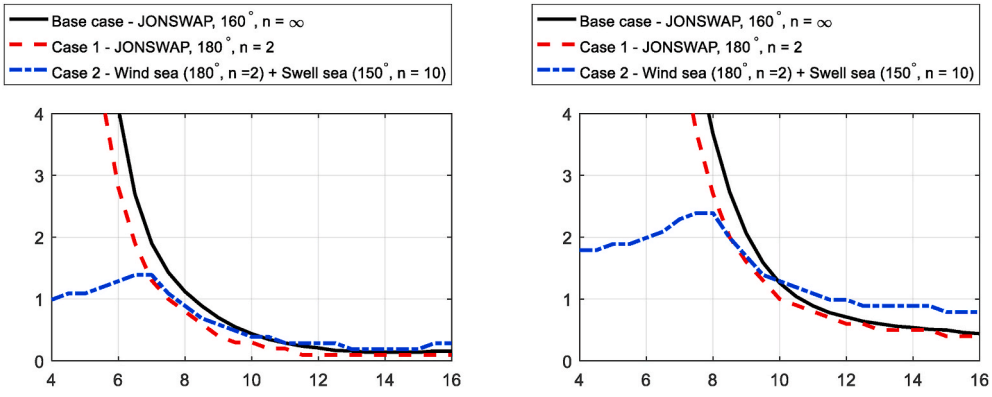

Fig. 11. Allowable sea states for the three chosen cases.

Table 4
Comparison of ratios for H_s limits with the recommended α-factor from DNVGL.

Vessel type	H_s ratios	T_p (s)				
		6	8	10	12	14
Mono-hull	Case1/Base case	***0.66***	***0.63***	***0.68***	***0.48***	0.71
	Case2/Base case	***0.32***	0.79	0.89	1.38	1.36
	DNVGL α-factor	0.87	0.73	0.72	0.72	0.72
Semi-submersible	Case1/Base case	0.90	***0.71***	0.79	0.85	0.93
	Case2/Base case	***0.18***	***0.65***	1.02	1.39	1.65
	DNVGL α-factor	0.87	0.86	0.75	0.72	0.72

The Hs ratios, which are less than the corresponding alpha factors are bolded in the table.

Fig. 11. As discussed earlier, the H_s limits drop significantly in short wave periods when considering both wind sea and swell sea components separately. The allowable H_s limits for Case 2 are highest when T_p is higher than 10 s, especially for the semi-submersibles. In general, the H_s limits are very low for T_p over 10 s: below 0.5 m for mono-hull and below 1 m for semi-submersibles for most cases. However, too much attention should not be given to the absolute values for the various cases, because the operational criterion applied is an example case. The focus here is the relative differences between these cases.

Since alpha factors are the only consideration in the current practice, it is interesting to check whether the alpha factors applied on the base case results can include the uncertainties in the allowable sea states due to different sea states modelling methods. In practice, the alpha factors are applied to reduce the H_s limits obtained from the planning phase, Hs_{Lim}, to increase the safety level during execution.

$$Hs_{WF} = \alpha \times Hs_{Lim} \tag{16}$$

where the alpha factor, $0 < \alpha < 1$, depends on the planed operation period, Hs_{Lim} , the forecast levels and whether or not meteorologists or wave measurements are available on site [1]. Hs_{WF} is the forecasted H_s limit that will be used for execution of the operation. To compare with the alpha factors, H_s ratios of Case 2 and Case 3 with respect to the base case are calculated. The results for both vessels are presented in Table 4 for five T_p conditions. Alpha factors from DNVGL recommended practice corresponding to 'Level A with meteorologist at site' for operation duration less than 12 h are used. Because alpha factors do not depend on T_p, the factors for T_p larger than 10 s are very close to each other due to low H_s variations.

From Table 4, it is seen that the needed alpha factors deviate significantly with the calculated H_s ratios. The H_s ratios, which are less than the corresponding alpha factors are bolded in the table. These conditions indicate that the alpha factors are not conservative enough to include the uncertainties due to the different sea state modeling methods compared to the base case. The largest deviations are found for Case 2 in short T_p conditions, where the H_s ratios are much lower than the suggested alpha factors. This reflects that if the real sea states contain wind sea and swell sea components from different directions, the simplified model used in the base case will provide too high estimate of the H_s limits even with alpha factors implemented. The consequence may be severe if the execution decision is made based these values. Thus, extra safety factors need to be considered to cover the sea state modelling uncertainties to lower the H_s limits. In longer waves, the alpha factors for most cases are lower than the calculated ratios. This indicate the alpha factors can cover the associated uncertainties for those conditions.

From the above comparison, it is suggested to improve the sea states modelling based on the actual site condition when assessing the allowable sea states in the planning phase. Otherwise, the alpha factors may not be able to cover the uncertainties from the simplified analysis with inaccurate sea state description.

5. Operability analysis

The previous section shows that the wave spectral type, spreading, and misalignment of the wind sea and swell sea have different influences on the allowable sea states. The influences also differ for the two vessel types. When planning the operations, it is of utmost importance to estimate the operability for the target location. In this section, a reference site in the Barents Sea is considered for the case study to compare the influences of the studied parameters on the operability. The same operation and operational criterion as described in Section 3 are used in the operability analysis.

5.1. Wave condition at the reference site

The hindcast wave data of one reference site at Barents Sea is chosen for the operability analysis. The coordinate of this site is [72.02°N, 22.1°E] with water depth around 350 m, and the location is illustrated in Fig. 12. The hindcast data are from the Norwegian Reanalysis Archive 10 km (NORA10) database providing wind and sea states characteristics every 3 h from September 1957 to present. NORA10 is a regional hindcast for the northeast Atlantic, including the North Sea, the Norwegian Sea and the Barents Sea, developed by the Norwegian Meteorological Institute based on the atmospheric downscaling of the European Reanalysis project (ERA-40) [24]. The NORA10 hindcast data has been validated and shown reasonably good agreement with offshore measurement data [25]. The data used in this study is 10-year wave data from 2003 to 2012, with 3-h resolution in time. The hindcast wave data provide statistics of H_s, T_p and wave direction for total sea, wind sea and swell sea.

Fig. 13 presents the scatter of the H_s and T_p of the wave data in January and July. The total sea, as well as the wind sea and swell sea components are displayed in the same figure. Although there are overlapping of these scatter plots, the swell seas are in general less steep with longer period than the wind seas. The extreme wave conditions with high H_s values are often dominant by the wind seas. For marine operations that are carried out in moderate and low sea states, wind sea and swell often occur simultaneously and can also be of comparable H_s level. In addition, the scatter plot of the two months clearly shows the higher possibility of severe wave conditions in the winter than in the summer, indicating the large deviation of the operability of the lifting operation for different months.

To better compare the wind sea and swell sea components for operational sea states, the wave conditions with total sea $H_s < 2.5\ m$ are chosen. Fig. 14 shows the relationship between H_s values for the two wave components for the chosen sea states. There is clear evidence that both swell sea and wind sea are significant, indicating the importance to model both components for marine operations. The mean and maximum H_s for swell sea decreases with increasing mean H_s for wind seas, especially in January. Moreover, the mean H_s for swell sea are lower in July, especially for low wind sea conditions.

The direction differences between simultaneous wind sea and swell sea are obtained for the chosen conditions and the distributions are presented in Fig. 15. The distribution shows the high possibility of having misalignment angle larger than 30 deg between the two components. However, it is also important to combine the relative wave heights of the two components with the direction misalignment. The most critical conditions correspond to the situations when both wave components can induce large motions for the installation vessel, and the misalignment is high. In such case, it is essential to choose the proper heading of the vessel to minimize the

Fig. 12. Location of the installation site (from Google Maps).

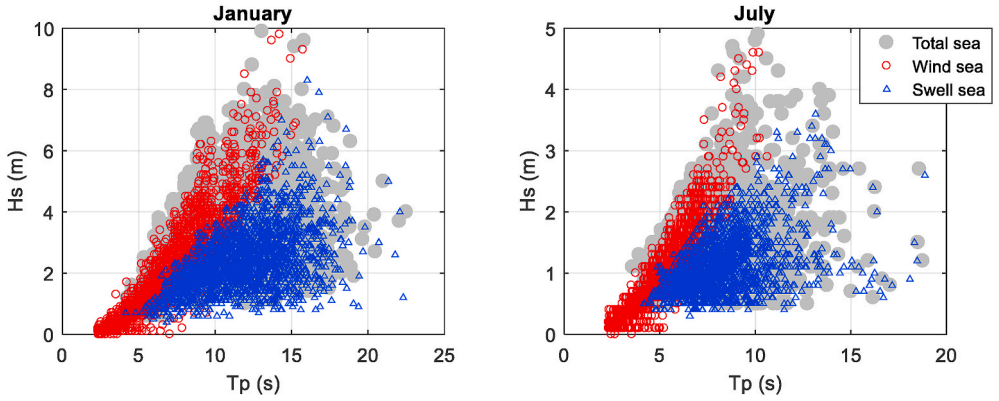

Fig. 13. Scatter plot of H_s and T_p for total sea, wind sea and swell sea components for the reference site.

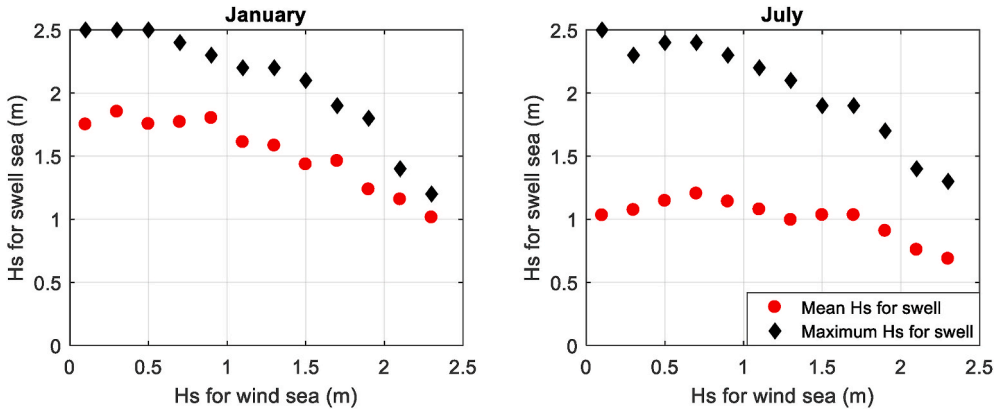

Fig. 14. Mean and maximum H_s of swell sea for given wind sea H_s (for conditions with total sea $H_s < 2.5\,m$).

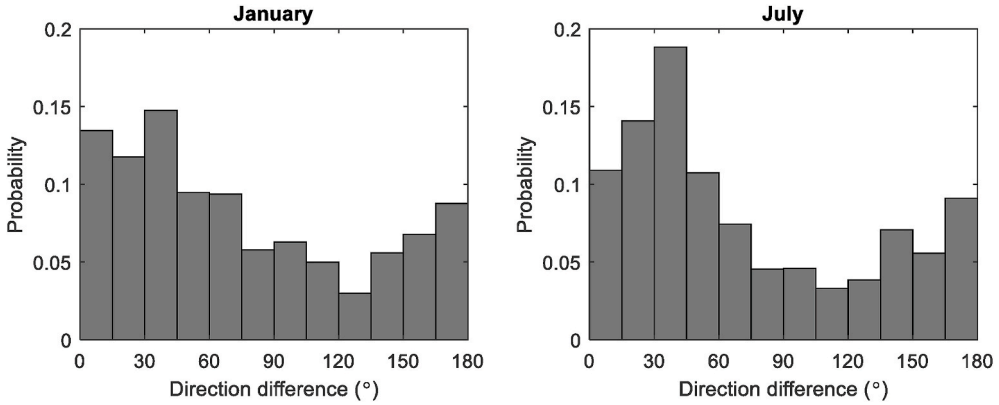

Fig. 15. Distribution of the direction difference between sea and swell sea components for conditions with total sea $H_s < 2.5\,m$.

crane tip motions.

5.2. Comparison of operability

The operability of an operation is defined as the ratio between the length of the workable weather windows and the total reference duration. The most critical phase of the lifting operation is assumed to last for 3 h. For each 3-h wave condition, knowing the wave statistics from the hindcast data, the response spectra and the STD values for the vertical crane tip motions can be calculated following

the procedure from Eqs. (4)–(6). By comparing the STD values with the limiting STD by Eq. (14) based on the operational criterion, it is found if this wave condition is allowable or not. Repeating this process for all the 10 years' hindcast data, the corresponding operability for this site can be estimated. Because there exists strong seasonal variability, operability for each month of the year are calculated separately.

First, the statistics of the total seas are used for the operability analysis to study the influence of the wave direction and spectral type. Fig. 16 presents the operability for two vessels using JONSWAP and Torsethaugen spectra, respectively. Three directions for the total sea with a spreading index of $n = 2$ are applied for all cases. It should be noted that the operations are often carried out with wave directions close to the heading sea condition. The operability under beam sea condition are presented only for comparison purpose.

For the mono-hull installation vessel, it is obvious that the operability are very sensitive to wave directions. The averaged operability in the summer months (May to August) using JONSWAP are 50.4%, 37.6% and 15.6%, respectively for the mono-hull vessel for heading of 180 deg, 150 deg and 90 deg. When using Torsethaugen to model the total wave spectrum, the resulting operability drop by around 13% for the summer months for 180 deg and 150 deg, and the variations of the operability over the months are higher. The operability in the winter seasons (November to February) are on average less than 4% for all directions. The decrease of the operability when using the two-peak spectrum compared to the single-peak spectrum are consistent with the allowable sea states that have been discussed in Section 4.

The influence of the heading on the operability are much less for the semi-submersible vessel compared to the mono-hull vessel. Compared to 180 deg, the averaged decrease of operability for summer months are around 7% and 25% for 150 deg and 90 deg, respectively. The less sensitivity with wave directions for the semi-submersible is because that the allowable sea states are higher for the same installation task compared to using the mono-hull vessel. The other reason is that the RAOs of the crane tip motion are less sensitive to wave directions than the mono-hull, as shown in Fig. 3.

The Torsethaugen spectrum is a good option when not much information is available about the nature of two-peaked spectra at a given location. However, limitations do exist on the analytical spectra when they are applied for operability analysis, since they represent average conditions [26,27]. Fig. 17 and Fig. 18 present the distribution of H_s and T_p for wind sea and swell sea components, respectively, based on the hindcast data at the reference site. Only the wave conditions with total sea H_s and T_p in the range of $1.75\ m < H_s < 2.25\ m$ and $5.5\ s < T_p < 6.5\ s$ are selected to obtain the distribution. The wind sea and swell sea parameters based on Torsethaugen spectrum (TH) with three different total sea H_s and T_p values are calculated and compared in the same figures. It can be

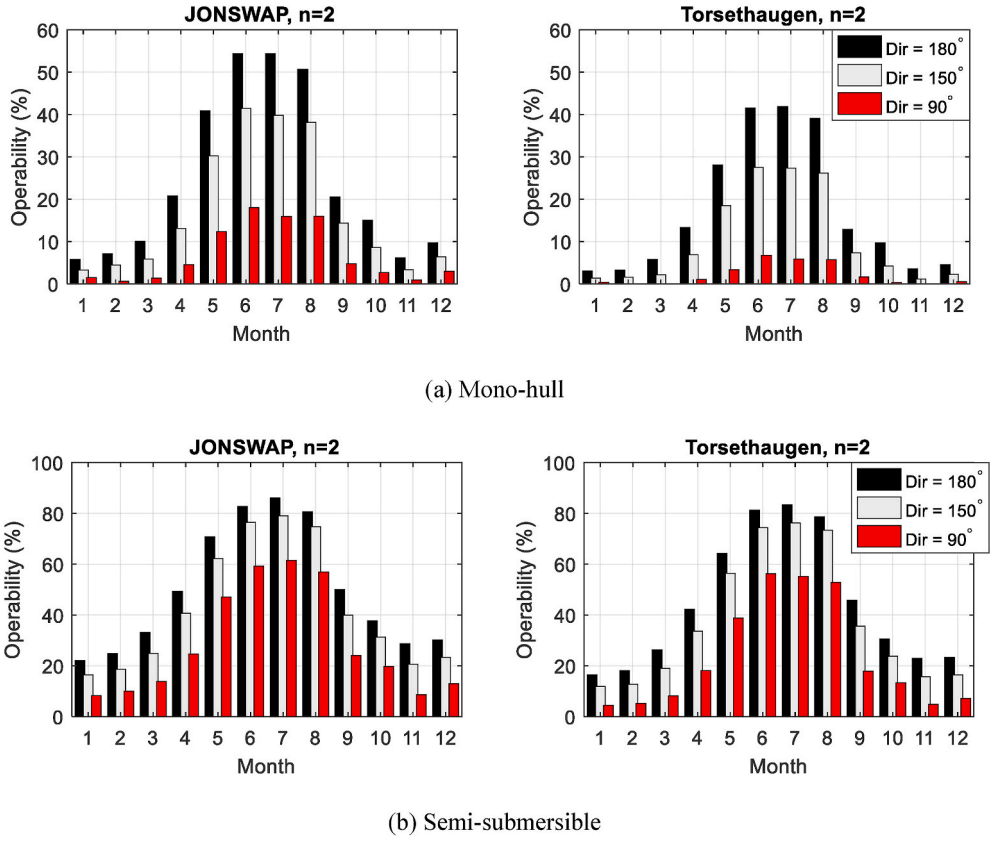

Fig. 16. Operability using total sea (spreading index $n = 2$).

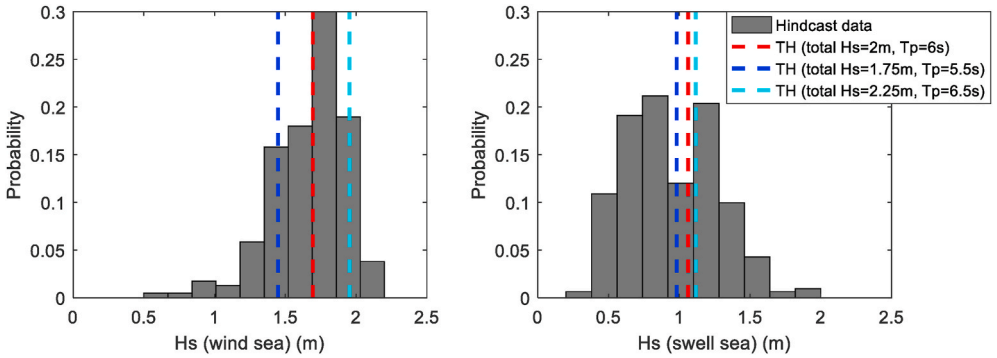

Fig. 17. Distribution of the wind sea and swell sea H_s values based on the hindcast data (the wave conditions for total sea with $1.75\,m < H_s < 2.25\,m$ and $5.5\,s < T_p < 6.5\,s$ are selected for this distribution).

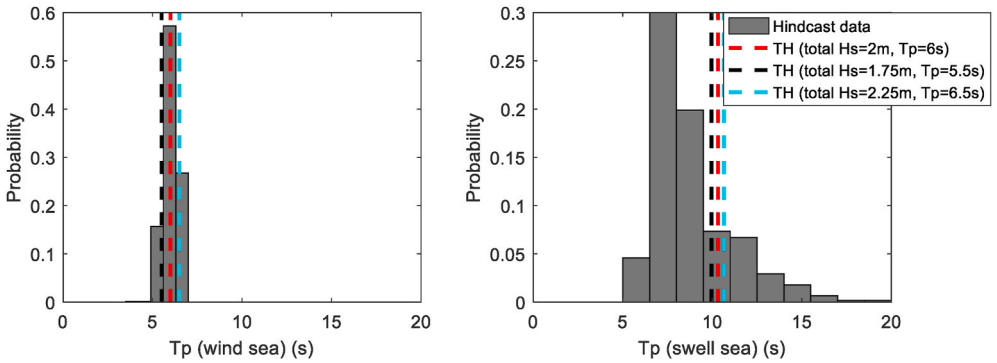

Fig. 18. Distribution of the wind sea and swell sea T_p values based on the hindcast data (the wave conditions for total sea with $1.75\,m < H_s < 2.25\,m$ and $5.5\,s < T_p < 6.5\,s$ are selected for this distribution).

observed that, except the wind sea T_p, the other three parameters are rather scattered. Although Torsethaugen can capture the mean H_s and T_p values for the two components, it cannot provide the uncertainties of the parameters for the same total sea condition. Thus, in the operability analysis considering wind sea and swell sea components, we directly use the hindcasted wind sea and swell sea characteristics.

Three scenarios for the vessel headings are compared by considering wind sea (with spreading index $n = 2$) and swell sea (with spreading index $n = 10$) separately when calculating the operability: 1) the wind sea and swell sea components are assumed to be aligned and both directions are 180 deg; 2) the vessel is always heading to the wave component with higher H_s values, and the wave direction of the other component is based on the misaligned angle between the two components from the hindcast data; 3) the vessel is always heading to the wind sea component, and the swell direction is based on the misaligned angle between the two components from the hindcast data. The operability of the above three scenarios using the separate wave components are also compared with those using the total sea modelled by Torsethaugen with $n = 2$, and the results are presented in Fig. 19.

For the operability of the mono-hull vessel shown in Fig. 19 (a), when using separate components and both propagating in 180 deg, the operability are much higher than using total sea modelled by Torsethaugen with the same heading. This is because that both the wind sea and swell sea components in the Torsethaugen use spreading index $n = 2$, and this will result in much higher responses of the crane tip compared to using $n = 10$ for the swell sea component in the separate case. When direction misalignment of the wave components is considered, the operability reduces. Compared to the aligned condition, the reduction of the operability when heading to the larger H_s component is limited, with an average of 4% for the summer months. However, the reduction when always heading to the wind sea component are much larger and around 14% on average. Thus, if the vessel responses are very sensitive to swells, it is not recommended to always head to the wind seas.

For the semi-submersible vessel, the operability are in general 30% higher than the same case using the mono-hull vessel. Because of the high allowable H_s values and the calm sea states in summer seasons, the differences of the resulting operability using different spectrum and heading scenarios are much less compared to the mono-hull vessel. However, the differences are still noticeable for the less favorable months in the year. Thus, the sensitivity of the operability with the wave spectral models and directions also highly depend on the vessel type.

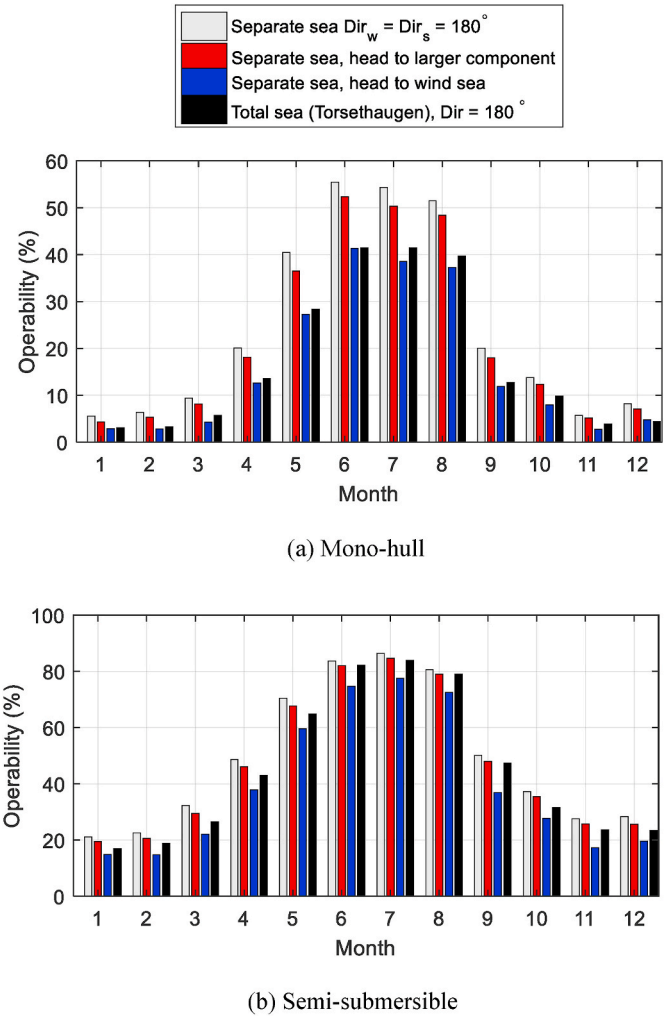

Fig. 19. Operability using total sea and separate wind sea and swell sea components. For separate cases, the spreading indices $n = 2$ and 10 are used for wind sea and swell sea, respectively.

6. Conclusions

This paper focuses on a case study of a typical lifting operation with the purpose to address the uncertainties of the operational limits due to different sea states modelling methods. The vertical crane tip motion is considered as the critical parameter to assess the allowable sea states. The influence of wave spreading, wave spectral type, as well as direction misalignment of wind sea and swell sea on the allowable sea states are compared. Two types of installation vessels are used for all the case studies. Operability analysis of such operation are performed using hindcast data for a reference site in the Barents Sea. The main conclusions from this study are drawn as follows:

- The response spectra of the crane tip vertical motions are sensitive to the spectral models used in the analysis. The response spectra tends to concentrate the density towards the swell sea direction. The allowable H_s values for both vessels are significantly less using Torsethaugen spectrum than using JONSWAP spectrum when T_p is less than 9 s. The inclusion of spreading of the waves provide conservative estimates on the operational limits compared to using long-crested waves.
- The H_s ratios based on three representative cases are calculated and compared with the alpha factors from the recommended practice. Alpha factors cannot cover the uncertainties due to sea state modelling for many conditions, and it is recommended to improve the sea state modelling in the planning phase based on actual sites to reduce the uncertainties in the allowable sea states.
- The hindcast wave data from the reference site shows high probability of direction misalignment between the wind sea and swell sea components. The data also indicate that the analytical spectra cannot well describe both wind sea and swell sea components for individual sea states, as well as their direction differences. To provide a better estimation of operability, it is recommended to use separate wind sea and swell sea in the sea state modelling and position the vessel to head to the sea component with higher H_s value.

- When comparing the behavior of the two vessels in the case study, the motion responses of the semi-submersible are much lower compared to those of the mono-hull vessel under the same condition, resulting in higher allowable sea states and operability. However, it should be mentioned that the cost of the vessels are significantly different. The choice of vessel needs to consider different practical aspects, in addition to the operability.

This study presents the case study using frequency-domain methods based on linear assumptions. For more complicated marine operations, dynamic time-domain analysis may be required to capture nonlinear responses. However, to assess the allowable sea states and estimate the operability using time-domain methods will be very time-consuming. More sophisticated models with less computational costs are essential to assess the operability for complicated marine operations. Moreover, the joint probabilistic models of wind sea and swell sea components based on long-term hindcast data can be established. The joint probabilistic models are often applied to find extreme conditions for design purpose. It is interesting to apply the joint probabilistic models and Monte Carlo simulations to study the uncertainties in the allowable sea states and operability. Future work can be devoted to study these aspects.

Declaration of competing interest

The authors declare that they have no known competing financial interests or personal relationships that could have appeared to influence the work reported in this paper.

Acknowledgment

The authors acknowledge Magnar Reistad from Norwegian Meteorological Institute for providing the NORA10 hindcast data for the reference site. The cooperation between University of Stavanger and Gubkin Russian State University of Oil and Gas through DIKU UTFORSK Project (project number UTF-2017-four-year/10044) is also acknowledged.

Appendix A

A.1 Wave spectral types

There are several analytical wave spectrum models that are widely used for design of marine operations. The most used spectra on the Norwegian Continental Shelf are Pierson-Moskowitz wave spectrum (PM), JONSWAP wave spectrum, and Torsethaugen wave spectrum.

PM spectrum is often used to describe a fully develop sea by the following equation [13]:

$$S_{PM}(\omega) = \frac{5}{16} H_S^2 \omega_p^4 \, \omega^{-5} \exp\left(-\frac{5}{4}\left(\frac{\omega}{\omega_p}\right)^{-4}\right) \tag{17}$$

where $\omega_p = \frac{2\pi}{T_p}$ is angular spectral peak frequency. The JONSWAP spectrum is formulated as a modification of the PM wave spectrum for a growing wind sea in a fetch limited situation [19]:

$$S_J(\omega) = A_\gamma S_{PM}(\omega) \gamma^{\exp\left(-0.5\left(\frac{\omega-\omega_p}{\sigma\omega_p}\right)^2\right)} \tag{18}$$

where $S_{PM}(\omega)$ is the PM spectrum; $A_\gamma = 1 - 0.287\, ln(\gamma)$, is a normalizing factor ensuring that correct variance of surface process is obtained for various values of γ; γ is the spectral peak parameter. Default values for spectral width parameter, σ are: $\sigma = 0.07$ for $\omega \leq \omega_p$, and $\sigma = 0.09$ for $\omega \geq \omega_p$. For low and moderate wind seas which are of interest for most marine operations, a likely range for γ is 1–3. To have a peak parameter larger than 3 will require strong wind, i.e., conditions not adequate for marine operations. For $\gamma = 1$, the JONSWAP spectrum reduces to the PM spectrum.

It is well-known that in many offshore areas, including the North Sea, real seas are often a combination of wind seas and swell seas. Such multi-modal wave spectra can result in unexpected vessel responses if the underlying spectral shape is not adequately described. The Torsethaugen two-peak spectrum is obtained by fitting two generalized JONSWAP functions to averaged measured spectra for a number of sea state classes based on wave measurements from the Northern North Sea [15]. Input parameters to the Torsethaugen spectrum are H_s and T_p. The spectral parameters are related to H_s and T_p by empirical functions established during the fitting process.

The Torsethaugen spectrum is given as a sum of wind sea spectrum and swell sea spectrum:

$$S_T(\omega) = \sum_{j=1}^{2} S_j(\omega) \tag{19}$$

where $j = 1$ corresponds to the primary sea system and $j = 2$ refers to the secondary sea system. The dominant condition (wind sea or swell sea) is determined by comparing T_p with the following defined period:

$$T_{pf} = a_f \cdot H_s^{1/3} \tag{20}$$

If $T_p > T_{pf}$, the primary spectral peak corresponds to the swell system, otherwise primary spectral peak corresponds to the local wind sea system. The factor a_f depends on the fetch length. For a fetch length of 370 km, a_f is 6.6 $s/m^{1/3}$ and for $H_s = 2\ m$ we find $T_{pf} = 8.1\ s$, so a sea state characterized be $H_s = 2\ m$ and $T_p = 6\ s$ will be dominated by the wind sea. Regarding detailed formulation of the two wave spectrum components, reference is made to Refs. [15,19].

Fig. 20 compares the PM, JONSWAP and Torsethaugen spectra for two sea states with different spectral peak periods. For both sea states, JONSWAP spectrum results in higher peaks than the other two spectra. Under shorter wave condition ($T_p = 6\ s$), in addition to the peak at 6 s, Torsethaugen shows a secondary peak at period around 10s, representing the expected swell sea condition. The separation of the Torsethaugen into wind sea and swell sea components for $T_p = 6\ s$ condition is illustrated in Fig. 21 where the two wave components are modelled using standard JONSWAP spectrum with $\gamma = 3.3$. As can be seen, although swell sea component is secondary, it still represents around 30% of the total wave energy. If the vessel is sensitive to long waves, the swell sea can produce much larger motions than the wind sea component, depending to some extent on the direction of propagations of the two wave systems relative to ship heading.

It should be noticed that Torsethaugen spectrum utilizes equal direction of propagation of wind sea and swell sea. This is because the data to which the Torsethaugen spectrum was fitted did not provide directional information. In practice, however, the wind sea normally follows close to the wind direction, while the swell system may come from another direction exposed to incoming sea from distant areas. One way to account for the direction misalignment is to decompose the two components of the Torsethaugen spectrum and apply two different directions. If measurement or hindcast data are available, the statistics of the two wave components are normally provided, and they can be modelled separately. The influence of the misalignment of the wave direction of the two components will be discussed when assessing allowable sea states and operability using the hindcast data.

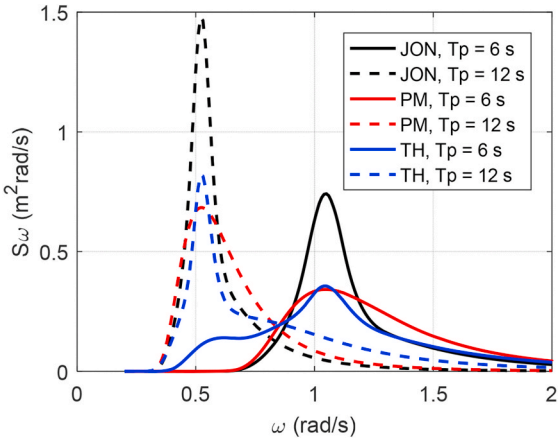

Fig. 20. Comparison between Torsethaugen (TH), JONSWAP (JON) and PM spectra ($H_s = 2\ m$).

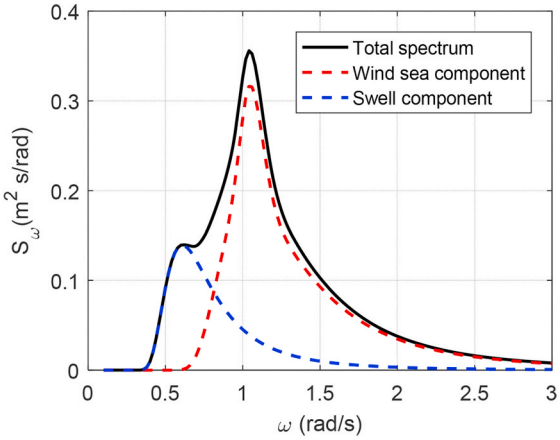

Fig. 21. Decomposition of Torsethaugen spectrum into two JONSWAP spectra (total sea: $H_s = 2\ m$, $T_p = 6\ s$; wind sea component: $H_{s1} = 1.69\ m$, $T_{p1} = 6\ s$; swell sea component: $H_{s2} = 1.06m$, $T_{p2} = 10.3s$).

A.2 Directional short-crested waves

The wave spectra discussed above are based on long-crested waves, in which the spectrum is only considered as functions of frequency ω. In the real sea condition, waves are typically short-crested, especially for the wind-generated seas. The directional spreading of wave energy may give rise to forces and motions that are different from those corresponding to long-crested waves. If long-crested waves are propagating in the worst direction regarding the response under consideration, short-crested seas will reduce the response. For other directions of propagation, short-crested waves may worsen the response.

A short-crested sea can be characterized by a two-dimensional wave spectrum, which is a function of both direction θ and frequency ω:

$$S(\omega,\theta) = S(\omega)\cdot D(\theta,\omega) \tag{21}$$

where $D(\theta,\omega)$ is the directional spreading function, which in general varies with frequency. Often, the frequency dependence is neglected and $D(\theta)$ can be approximated by the following equation [19]:

$$D(\theta) = \begin{cases} C(n)\cdot cos^{n}(\theta-\theta_0), & |\theta-\theta_0| \le \pi/2 \\ 0. & |\theta-\theta_0| > \pi/2 \end{cases} \tag{22}$$

where θ_0 is the mean wave direction of propagation about which the angular distribution is centered. The parameter n is a spreading index describing the degree of wave short-crestedness with $n \to \infty$ representing a long-crested wave field. $C(n)$ is a normalized constant ensuring the integration of $D(\theta)$ over θ equals 1 and is given by:

$$C(n) = \frac{1}{\sqrt{\pi}}\frac{\Gamma(1+n/2)}{\Gamma(1/2+n/2)} \tag{23}$$

where Γ denotes the Gamma function. Consideration should be taken to reflect an accurate correlation between the actual sea state and the index n. Therefore, with a sea state composing of both wind sea and swell sea, it is reasonable to separate these two components and use different spreading indices. Typical values for the spreading index for wind generated sea are $n = 2$ to $n = 4$. If used for swell, $n \ge 6$ is more appropriate [19].

References

[1] DNVGL. Standard DNVGL-ST-N001, Marine operations and marine warranty. Oslo, Norway: DNV GL AS; 2016.
[2] Li L. Marine operations. In: Cui W, Fu S, Hu Z, editors. Encyclopedia of ocean engineering. Singapore: Springer; 2020. https://doi.org/10.1007/978-981-10-6963-5_194-1.
[3] Li L. Dynamic analysis of the installation of monopiles for offshore wind turbines. PhD thesis. Department of Marine Technology, Norwegian University of Science and Technology; 2016. p. 1–70.
[4] Guachamin Acero W, Li L, Gao Z, Moan T. Methodology for assessment of the operational limits and operability of marine operations. Ocean Eng 2016;125:308–27.
[5] Gao Z, Guachamin-Acero W, Li L, Zhao Y, Li C, Moan T. Numerical simulation of marine operations and prediction of operability using response-based criteria with an application to installation of offshore wind turbine support structures. In: Marine operations specialty symposium (MOSS 2016); 2016.
[6] Solaas F, Sandvik PC, Påkozdi C, Kendon T, Larsen K, Myhre E. Dynamic forces and limiting sea states for installation of grp protection covers. In: International conference on offshore mechanics and arctic engineering, vol. 57779. American Society of Mechanical Engineers; 2017. V009T12A032.
[7] Li L, Parra C, Zhu X, Ong MC. Splash zone lowering analysis of a large subsea spool piece. Mar Struct 2020;70:102664.
[8] ISO. Ships and marine technology - offshore wind energy - port and marine operations. Geneva, Switzerland: International Organization for Standardization; 2015. ISO 29400.
[9] Natskår A, Moan T, Alvær PØ. Uncertainty in forecasted environmental conditions for reliability analyses of marine operations. Ocean Eng 2015;108:636–47.
[10] De Girolamo P, Di Risio M, Beltrami GM, Bellotti G, Pasquali D. The use of wave forecasts for maritime activities safety assessment. Appl Ocean Res 2017;62:18–26.
[11] Wilcken S. Alpha factors for the calculation of forecasted operational limits for marine operations in the Barents Sea. Norway: Master's thesis, University of Stavanger; 2012.
[12] Hasselmann K, Barnett TP, Bouws E, Carlson H, Cartwright DE, Enke K, Ewing JA, Gienapp H, Hasselmann DE, Kruseman P, Meerburg A. Measurements of wind-wave growth and swell decay during the Joint North Sea Wave project (JONSWAP). Ergänzungsheft 1973:8–12.
[13] Pierson Jr WJ, Moskowitz L. A proposed spectral form for fully developed wind seas based on the similarity theory of SA Kitaigorodskii. J Geophys Res 1964;69(24):5181–90.
[14] Ochi MK, Hubble EN. On six-parameters wave spectra". In: Proceeding of 15th coastal eng. Conference, vol. 1; 1976. p. 301–28.
[15] Torsethaugen K, Haver S. Simplified double peak spectral model for ocean waves. In: Proceedings of the 14th international offshore and polar engineering conference, toulon, France, may 23-28, 2004; 2004.
[16] Guachamin Acero W, Li L. Methodology for assessment of operational limits including uncertainties in wave spectral energy distribution for safe execution of marine operations. Ocean Eng 2018;165:184–93.
[17] Papoulis A, Pillai SU. Probability, random variables, and stochastic processes. Tata McGraw-Hill Education; 2002.
[18] Haver S, Moan T. On some uncertainties related to the short term stochastic modelling of ocean waves. Appl Ocean Res 1983;5(2):93–108.
[19] DNVGL. Recommended practice DNVGL-RP-C205, Environmental conditions and environmental loads. Oslo, Norway: DNVGL AS; 2017.
[20] Li L, Gao Z, Moan T. Response analysis of a nonstationary lowering operation for an offshore wind turbine monopile substructure. J Offshore Mech Arctic Eng 2015;137(5).
[21] Zhao Y, Cheng Z, Gao Z, Sandvik PC, Moan T. Numerical study on the feasibility of offshore single blade installation by floating crane vessels. Mar Struct 2019;64:442–62.
[22] DNV. Wave analysis by diffraction and Morison theory. SESAM user manual. Oslo, Norway: DNV; 2010.
[23] DNVGL. Recommended practice DNVGL-RP-H103, Modelling and analysis of marine operations. Oslo, Norway: DNVGL AS; 2014.

[24] Reistad M, Breivik Ø, Haakenstad H, Aarnes OJ, Furevik BR, Bidlot JR. A high-resolution hindcast of wind and waves for the North Sea, the Norwegian Sea, and the Barents Sea. J Geophys Res: Oceans 2011;116(C5).
[25] Bruserud K, Haver S. Comparison of wave and current measurements to NORA10 and NoNoCur hindcast data in the northern North Sea. Ocean Dynam 2016;66 (6–7):823–38.
[26] Bitner-Gregersen EM. Joint met-ocean description for design and operations of marine structures. Appl Ocean Res 2015;51:279–92.
[27] Bitner-Gregersen EM, Toffoli A. Uncertainties of wind sea and swell prediction from the Torsethaugen spectrum. In: ASME paper No. OMAE2009-80261, proc. Of the ASME 28th international conference on ocean and arctic engineering, honolulu, Hawaii, USA, may 31-june 5, vol. 2; 2009. p. 851–8.